Colloque lancement du GDR ADN

Nouveaux outils de simulation pour la modélisation des chromosomes

Equipe M3V du LPTMC

Pascal Carrivain (doctorant), Maria Barbi, Axel Cournac (post-doc), Annick Lesne, Julien Mozziconacci, Laurence Signon, Jean-Marc Victor

Laboratoire de Physique Théorique de la Matière Condensée, Université Pierre et Marie Curie, 4, Place Jussieu, 75252 Paris Cedex 05, France

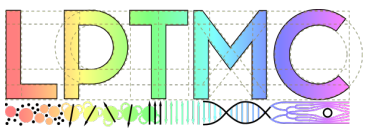

4 mai 2012

Sommaire

Cranshaft et méthode du pivot (1)

DNA Extension under the Action of an External Force

Alexander Vologodskii[†]

Department of Molecular and Cell Biology, University of California, Berkeley, California 94720

Received March 23, 1994; Revised Manuscript Received July 11, 1994[⊗]

ABSTRACT: We computed the extension–force dependence for the wormlike model of a polymer chain. The dependence that we obtained differs essentially from the corresponding well-known dependence for the freely jointed chain when the extension exceeds half of the chain contour length. We used the computed results to analyze the measurements of extension of individual DNA molecules under the action of force made recently (Smith, S. B.; Finzi, L.; Bustamante, C. *Science* **1992**, *258*, 1122). We took into account the electrostatic interaction between DNA segments for a very low salt concentration. The theoretical dependencies obtained are in very good agreement with the experimental data.

Cranshaft et méthode du pivot (2)

II. Models and Methods of Computations

A polymer chain composed of n Kuhn statistical segments was modeled as a chain consisting of mn rigid straight segments of equal size. The elastic energy of the chain, E_b, was computed as

$$E_b = kT\alpha \sum_{i=1}^{mn-1} \theta_i^2 \qquad (1)$$

where the summation is done over all of the joints between the rigid segments, α is the bending rigidity constant, and θ_i is the angular displacement of segment i relative to segment $i+1$. The bending constant α is defined so that the Kuhn statistical length corresponds to m rigid segments.[6] This model is transformed into the wormlike chain model as m approaches infinity.

To simulate the extension of the model chain, we fixed one of its ends at point 0 and applied a force, F, directed along the x axis, to the second end. The total energy of a particular conformation, E, was:

$$E = E_b - xF \qquad (2)$$

where x is the x-coordinate of the second end of the chain.

Equilibrium sets of the chain conformations for different F values were constructed by the Metropolis procedure.[7] There were two types of chain displacement used in the procedure. In the first type, a subchain containing an arbitrary number of adjacent segments is rotated by a randomly chosen angle, ϕ^1, around the straight line connecting the vertices bounding the subchain. In the second type, a subchain containing an arbitrary number of segments and including the free end of the chain is rotated by a randomly chosen angle, ϕ^2, around a randomly oriented line passing through the internal end of the subchain. The values of ϕ^k were uniformly distributed over intervals, $(-\phi_0^k, \phi_0^k)$, chosen so that about half of the proposed moves of each type were accepted.

Most of the calculations were done for model chains consisting of 10 Kuhn statistical segments, but when checked, results were the same for 5 and 50 segments. For accuracy, up to 10^8 elementary displacements were produced for any particular values of F and m. The average value of x, $\langle x \rangle$, was calculated as the average through a particular set.

For the very low salt concentration, 10^{-4} M NaCl, we introduced the electrostatic interaction to the model in terms of the Debye–Hückel approximation. Although in general this approximation is not accurate enough to describe the electrostatic contribution to DNA bending rigidity,[8,9] at 10^{-4} M NaCl the approximation is satisfactory. The term E_{el} which we added to the chain energy was

$$E_{el} = \sum_i \sum_{j>i} \int\int \frac{\upsilon^2 \exp(-\kappa r)\, dr_i\, dr_j}{D r_{ij}} \qquad (3)$$

where υ is the effective linear charge density of DNA, κ is the Debye–Hückel screening parameter, D is the dielectric constant of water, and r_i is a point of chain segment i, $r_{ij} = r_i - r_j$. The sum here is over all couples of chain segments, and the integrals should be taken along the segments i and j. For [NaCl] = 10^{-4} M, the υ value should be very close to that predicted by condensation theory, 0.14 e/Å.[9,10] The bending rigidity constant corresponded to b = 100 nm. Changing this constant up to 30% did not alter the results significantly because the electrostatic interaction provides the main contribution to the bending rigidity at this salt concentration. Most of the simulated results for this model were obtained for m = 100 and chain length = 2000 nm. A total of 10^5 elementary displacements were produced for each point.

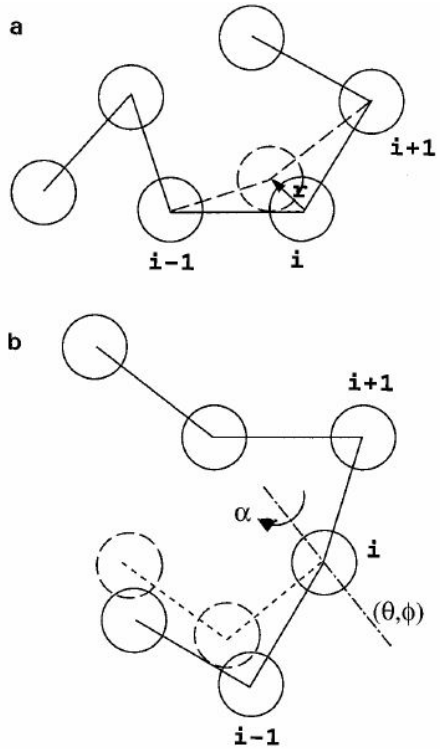

FIG. 1. Two types of Monte Carlo moves: (a) local, random bead displacement and (b) global, random axis rotation.

(a) (b) (c) Jian 1997

Bead spring model (1)

A Brownian Dynamics Program for the Simulation of Linear and Circular DNA and Other Wormlike Chain Polyelectrolytes

Konstantin Klenin, Holger Merlitz, and Jörg Langowski
Division Biophysics of Macromolecules, German Cancer Research Center, D-69120 Heidelberg, Germany

ABSTRACT For the interpretation of solution structural and dynamic data of linear and circular DNA molecules in the kb range, and for the prediction of the effect of local structural changes on the global conformation of such DNAs, we have developed an efficient and easy way to set up a program based on a second-order explicit Brownian dynamics algorithm. The DNA is modeled by a chain of rigid segments interacting through harmonic spring potentials for bending, torsion, and stretching. The electrostatics are handled using precalculated energy tables for the interactions between DNA segments as a function of relative orientation and distance. Hydrodynamic interactions are treated using the Rotne-Prager tensor. While maintaining acceptable precision, the simulation can be accelerated by recalculating this tensor only once in a certain number of steps.

Bead spring model (2)

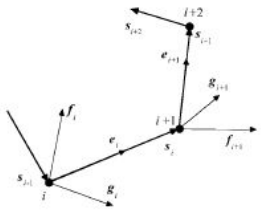

FIGURE 1 Chain geometry with the segment vectors s_i and the segment coordinate systems ($\mathbf{f}_i$, $\mathbf{g}_i$, $\mathbf{e}_i$) that define the relative orientation between segments.

The total energy of a given chain conformation is given as the sum of the stretching, bending, twist, and electrostatic energies.

The stretching energy is defined for each segment i:

$$\frac{E_i^{(s)}}{k_B T} = \frac{1}{2(l_0\delta)^2}(l_0 - s_i)^2 \tag{1}$$

Here k_B is the Boltzmann constant, T the temperature, l_0 the segment equilibrium length, and δ the stiffness parameter, so that $(l_0\delta)^2$ is approximately equal to the variance of the segment length distribution.

The bending energy is defined for each chain joint. We call a joint *unbent* if it connects segments that form a straight line at equilibrium, and *bent* if the angle θ_i^* between the segments at equilibrium is nonzero. To each bent joint i we attach an auxiliary unit vector b_i that is fixed in the coordinate system (f_i, g_i, e_i), its polar coordinates being $(\theta_i^*, \varphi_i^*)$. Note that this formalism is different from our first implementation (Chirico and Langowski, 1996) where a heuristic "kink potential" was used that was given in terms of the Euler angles for rotating one segment into the next. Here the bending energy of the ith joint is:

$$\frac{E_i^{(b)}}{k_B T} = \alpha_b \beta_i^2 \tag{2}$$

where β_i is the angle between e_{i-1} and e_i for an unbent joint, or between e_{i-1} and b_i for a bent joint; α_b is the bending rigidity parameter chosen in such a way that the Kuhn length is equal to:

$$B = l_0 \frac{1 + \langle \cos\beta \rangle}{1 - \langle \cos\beta \rangle}, \tag{3}$$

where

$$\langle \cos\beta \rangle = \frac{\int_0^\pi \cos\beta \sin\beta \exp(-\alpha_b\beta^2)d\beta}{\int_0^\pi \sin\beta \exp(-\alpha_b\beta^2)d\beta}.$$

The twist energy is defined for each adjacent segment pair:

$$\frac{E_i^{(t)}}{k_B T} = \frac{1}{2k_B T}\frac{C}{l_0}\tau_i^2, \tag{4}$$

where C is the torsional rigidity constant and τ_i is the twist angle between the $(i-1)$th and ith segments.

The twist angle τ_i is calculated by defining a vector $p_i = s_{i-1} \times s_i$, which is normal both to s_{i-1} and s_i. Now, we can easily calculate the angles α_i between f_{i-1} and p_i, and γ_i between p_i and f_i. Then, $\tau_i = \alpha_i + \gamma_i$ (Fig. 2). During the BD simulation we assume that at time t, $\tau_i(t - \Delta t) - \pi \le \tau_i(t) \le \tau_i(t - \Delta t) + \pi$, where $\tau_i(t - \Delta t)$ is the twist angle one simulation step ago (Δt is chosen such that the probability that the twist angle changes by more than $\pm\pi$ becomes negligible).

The starting point for the electrostatic energy is the expression for the energy of interaction between two uniformly charged nonadjacent segments (i, j) in a 1:1 salt solution in the Debye-Hückel approximation:

$$\frac{E_{ij}^{(e)}}{k_B T} = \frac{v^2}{k_B T D}\int d\lambda_i \int d\lambda_j \frac{\exp(-\kappa r_{ij})}{r_{ij}}. \tag{5}$$

The integration is done along the two segments; λ_i and λ_j are the distances from the segment beginnings, r_{ij} is the distance between the current positions at the segments to which the integration parameters λ_i and λ_j correspond; κ is the inverse of the Debye length, so that $\kappa^2 = 8\pi e^2 I/k_B T D$, I is the ionic strength, e the proton charge, D the dielectric constant of water, v the linear charge density which for DNA is equal to $v_{DNA} = -2e/\Delta$, where $\Delta = 0.34$ nm is the distance between basepairs.

There are two problems to be solved for the Eq. 5: 1) the linear density v should be renormalized from that of DNA to a smaller value in order to ensure the correct excluded volume effects; 2) the integration should be approximated by a more simple procedure to save computation time.

The renormalization of the linear density was done as in Stigter (1977). As pointed out in Schellman and Stigter (1977), the Gouy layer of immobile counterions reduces the effective charge density by a factor of $q = 0.73$ for NaCl concentrations between 1 and 500 mM. Next, the Debye-Hückel approximation is a linearization of the Poisson-Boltzmann equation and valid only for a very small electric potential: $\varphi \ll k_B T/e$. We choose the renormalized charge

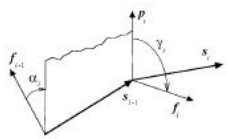

FIGURE 2 Definition of the twist angle $\tau_i = \alpha_i + \gamma_i$. $\mathbf{p}_i$ is perpendicular to $\mathbf{s}_{i-1}$ and $\mathbf{s}_i$; α_i is measured between $\mathbf{f}_{i-1}$ and $\mathbf{p}_i$, γ_i between $\mathbf{p}_i$ and $\mathbf{f}_i$.

density v^* in such a way that the known solution of the Debye-Hückel equation for a straight thin line with charge density v^* coincides with the solution of the Poisson-Boltzmann equation for a cylinder of the DNA radius r_{ES} and the charge density qv_{DNA} in the regions where $\varphi \ll k_B T/e$ (Fig. 3).

In order to save computation time, a tabulation of the double integral (Eq. 5) was used. For simplicity we assume that each segment has the same length l_0. For each segment pair (i, j) we can define a vector $l_0 R_{ij}$ connecting the middle points of the two segments. Then the mutual position of the segments can be defined by the following four dimensionless parameters:

$$\rho_{ij} = |R_{ij}|,$$

center-to-center distance in L_0 units, $\rho_{ij} \ge 0$ (6a)

$$\gamma_{ij} = (1/\rho_{ij})e_i \cdot R_{ij},$$

tilt angle cosine for the ith segment, $-1 \le \gamma_{ij} \le 1$ (6b)

$$\gamma_{ji} = -(1/\rho_{ij})e_j \cdot R_{ij},$$

tilt angle cosine for the jth segment, $-1 \le \gamma_{ji} \le 1$ (6c)

$$\sigma_{ij} = \frac{(e_i \times R_{ij}) \cdot (e_j \times R_{ij})}{|e_i \times R_{ij}||e_j \times R_{ij}|},$$

twist angle cosine, $-1 \le \sigma_{ij} \le 1$ (6d)

Equation 5 can be rewritten in the form:

$$\frac{E_{ij}^{(e)}}{k_B T} = \alpha_e f(\rho_{ij}, \gamma_{ij}, \gamma_{ji}, \sigma_{ij}) \tag{7}$$

where $\alpha_e = v^{*2} l_0/k_B T D$ and

$$f(\rho, \gamma_1, \gamma_2, \sigma) = \int_{-1/2}^{1/2} dx_1 \int_{-1/2}^{1/2} dx_2 \frac{\exp(-\kappa|R|)}{|R|}, \tag{8}$$

$$\mathbf{R} = \rho \mathbf{v}_0 - x_1 \mathbf{v}_1 + x_2 \mathbf{v}_2 \tag{9}$$

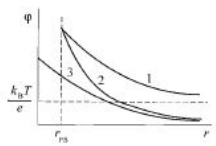

FIGURE 3 Electrostatic potential for the interaction between DNA segments. A Debye-Hückel potential (1) was renormalized (3) such as to coincide at large distances with the nonlinear Poisson-Boltzmann equation (2).

where $\mathbf{v}_0$, $\mathbf{v}_1$, and $\mathbf{v}_2$ are unit vectors oriented in such a way that $\mathbf{v}_0\mathbf{v}_1 = \gamma_1$, $-\mathbf{v}_0\mathbf{v}_2 = \gamma_2$, and $(\mathbf{v}_1 \times \mathbf{v}_0) \cdot (\mathbf{v}_2 \times \mathbf{v}_0)/|\mathbf{v}_1 \times \mathbf{v}_0||\mathbf{v}_2 \times \mathbf{v}_0| = \sigma$.

In the following we need the partial derivatives of Eq. 8. At first, a four-dimensional table for the values of the integral (Eq. 8) and each of its partial derivatives was constructed *numerically*. Then, during the simulation, a linear interpolation was used to obtain the values of $(\partial f/\partial\rho)$, $(\partial f/\partial\gamma_1)$, $(\partial f/\partial\gamma_2)$, $(\partial f/\partial\sigma)$ at particular points of the $(\rho, \gamma_1, \gamma_2, \sigma)$ space. The table steps were chosen in such a way that the values of ρ, arccos γ_1, arccos γ_2, and arccos σ had constant increments. The tabulation range for γ_1, γ_2, and σ is $[-1,1]$. The range of ρ, $[\rho_{min}\ \rho_{max}]$, and the table size for each argument are parameters of the approximation, which we chose by the following criteria. For the minimum distance, ρ_{min}, all possible values of the electrostatic energy should be large enough (e.g., $>10\ k_B T$), so that this distance is practically unreachable during the simulations. For distances $>\rho_{max}$ all possible energy values should be negligible (say, $<0.01\ k_B T$). The mutual displacement of segments corresponding to one ρ-step should not exceed the Debye length, and the same restriction is applied to the displacement of segment ends corresponding to one step in the γ_1, γ_2, and σ dimensions. These criteria are rather "soft," in order to keep the total table size within reasonable limits (the minimum table size for $l_0 = 10$ nm and $I = 1$ M is 14 MB of memory, including all partial derivatives of Eq. 8). We should note, however, that even crude hard-core potentials for electrostatic repulsion in DNA can be applied in many cases to predict statistical properties of DNA to good precision (Vologodskii and Cozzarelli, 1995); therefore, the representation of the electrostatic potential according to Eqs. 7 and 8 is probably a good approximation.

So far, we neglected the fact that the segment length is only approximately equal to l_0. That means that the "charged" segment does not coincide exactly with the "geometrical" segment. This seems to be a good approximation for the excluded volume effects, since the chain is supposed to be stiff with respect to stretching ($\delta \ll 1$). One has to be careful, however, to avoid that during the simulation parts of the chain cross each other through discontinuities between adjacent charged segments, if the length of their phantom geometrical counterparts is greater than l_0. In order to exclude this possibility we define the R_{ij} vector for two segments (i, j) of arbitrary length in the following way:

$$R_{ij} = \frac{1}{l_0}(r_{j(i)}^{(m)} - r_{i(j)}^{(m)}) \tag{10}$$

where $r_{i(j)}^{(m)}$ is a "shifted" middle point of the segment:

$$r_{i(j)}^{(m)} = \begin{cases} r_i + (l_0/2)e_i, & \text{if } |r_j^{(m)} - r_i| \le |r_j^{(m)} - r_{i+1}|; \quad (a) \\ r_{i+1} - (l_0/2)e_i, & \text{else;} \quad (b) \end{cases} \tag{11}$$

and $r_j^{(m)} = (r_j + r_{j+1})/2$ is the actual middle point of the segment. This means that the geometrical segment that is used to calculate the excluded volume interaction is shifted

(a) (b)

Bead spring model (3)

with its end toward the segment joint that is closest to the other segment in the interaction. Thereby, any gaps that might appear at the joint due to stretching are automatically closed and the chains cannot cross.

Since forces and torques are the partial derivatives of the energy over the system coordinates, the latter should be specified formally. For each segment i we chose the following four coordinates: the three space coordinates r_i of the segment beginning and the angle φ_i of rotation of the local vector basis (f_i, g_i, e_i) around the e_i axis. For the angle coordinate the zero position is not defined. Therefore, in addition, we need to specify how to keep the φ_i coordinates unchanged while a displacement of the r_i coordinates takes place. The following rule was used to derive forces and torques and to perform moves in the simulation procedure. If, as a result of r_i displacement, the e_i vector has a new value e_i' and A_i is a rotation matrix, so that $e_i' = A_i e_i$, then the new value of the f_i vector is $f_i' = A_i f_i$.

In a linear chain three additional degrees of freedom r_N are required for the last segment. Here are the expressions for the forces and torques for the ith segment obtained by differentiating Eqs. 1, 2, 4, and 7:

Stretching force

The stretching force acting on the ith vertex from the $(i + 1)$th one is parallel to the ith segment:

$$\frac{\mathbf{F}_{i,\mathrm{next}}^{(s)}}{k_B T} = \frac{s_i - l_0}{(l_0 \delta)^2}\,\mathbf{e}_i \tag{12}$$

The total stretching force for the ith vertex is therefore

$$\mathbf{F}_i^{(s)} = -\mathbf{F}_{i-1,\mathrm{next}}^{(s)} + \mathbf{F}_{i,\mathrm{next}}^{(s)} \tag{13}$$

Bending force

The contribution of the energy stored in the bending angle β_i to the bending force acting on the ith vertex from the $(i + 1)$th one is perpendicular to the ith segment and lies in the bend plane:

$$\frac{\mathbf{F}_{i,\mathrm{next}}^{(b)}}{k_B T} = \frac{2\alpha_b \beta_i}{s_i}\,\hat{\mathbf{p}}_i \times \mathbf{e}_i \tag{14a}$$

for an unbent joint, and

$$\frac{\mathbf{F}_{i,\mathrm{next}}^{(b)}}{k_B T} = \frac{2\alpha_b \beta_i}{s_i \sin\beta_i}\,(\mathbf{e}_{i-1} \times \mathbf{b}_i) \times \mathbf{e}_i \tag{14b}$$

for a bent joint. Here $\hat{\mathbf{p}}_i = \mathbf{p}_i/p_i$; $\mathbf{p}_i = s_{i-1} \times s_i$, so that $\hat{\mathbf{p}}_i = \mathbf{e}_{i-1} \times \mathbf{e}_i/\sin\beta_i^*$ where β_i^* is the angle between $\mathbf{e}_{i-1}$ and $\mathbf{e}_i$ (for an unbent joint, $\beta_i^* = \beta_i$).

The analogous contribution to the bending force acting on the ith vertex from the $(i - 1)$th one is perpendicular to the $(i - 1)$th segment and also lies in the bend plane:

$$\frac{\mathbf{F}_{i,\mathrm{prev}}^{(b)}}{k_B T} = \frac{2\alpha_b \beta_i}{s_{i-1}}\,\hat{\mathbf{p}}_i \times \mathbf{e}_{i-1} \tag{15a}$$

for an unbent joint, and

$$\frac{\mathbf{F}_{i,\mathrm{prev}}^{(b)}}{k_B T} = \frac{2\alpha_b \beta_i}{s_{i-1}\sin\beta_i}[\mathbf{b}_i - (\mathbf{e}_{i-1} \cdot \mathbf{b}_i)\mathbf{e}_{i-1}] \tag{15b}$$

for a bent joint.

Note that Eqs. 14a and 15a for an unbent joint are symmetric with respect to renumbering the vertices in opposite order (one force can be obtained from the other by substituting $s_i \leftrightarrow -s_{i-1}$, $\mathbf{e}_i \leftrightarrow -\mathbf{e}_{i-1}$, $\hat{\mathbf{p}}_i \leftrightarrow -\hat{\mathbf{p}}_{i-1}$). Obviously, there is no such symmetry for a bent joint because the $\mathbf{b}_i$ vectors are not defined in a symmetrical way. We note also that the expressions for a bent joint (14b, 15b) become those for the unbent joint upon substituting $\mathbf{b}_i \to \mathbf{e}_i$.

The total bending force for the ith vertex is

$$\mathbf{F}^{(b)} = -\mathbf{F}_{(i-1),\mathrm{next}}^{(b)} + \mathbf{F}_{i,\mathrm{prev}}^{(b)} + \mathbf{F}_{i,\mathrm{next}}^{(b)} - \mathbf{F}_{(i+1),\mathrm{prev}}^{(b)} \tag{16}$$

Bending torque

The torque on segment i induced by bending is for a bent joint:

$$\frac{T_i^{(b)}}{k_B T} = \frac{2\alpha_b \beta_i}{\sin\beta_i}\,\mathbf{e}_{i-1} \cdot (\mathbf{e}_i \times \mathbf{b}_i) \tag{17}$$

For an unbent joint, this torque is equal to zero.

Twisting force

The force on the ith vertex from the $(i + 1)$th one induced by mutual twisting of the $(i - 1)$th and ith segments by an angle τ_i is perpendicular to the plane of the ith bend:

$$\frac{\mathbf{F}_{i,\mathrm{next}}^{(t)}}{k_B T} = \frac{C}{k_B T l_0}\frac{\tau_i s_{i-1}}{p_i}(1 - \mathbf{e}_{i-1} \cdot \mathbf{e}_i)\hat{\mathbf{p}}_i \tag{18}$$

The symmetric expression for the twisting force acting on the ith vertex from the $(i - 1)$th one is

$$\frac{\mathbf{F}_{i,\mathrm{prev}}^{(t)}}{k_B T} = -\frac{C}{k_B T l_0}\frac{\tau_i s_i}{p_i}(1 - \mathbf{e}_{i-1} \cdot \mathbf{e}_i)\mathbf{p}_i \tag{19}$$

The total twisting force for the ith vertex is then

$$\mathbf{F}_i^{(t)} = -\mathbf{F}_{(i-1),\mathrm{next}}^{(t)} + \mathbf{F}_{i,\mathrm{prev}}^{(t)} + \mathbf{F}_{i,\mathrm{next}}^{(t)} - \mathbf{F}_{(i+1),\mathrm{prev}}^{(t)} \tag{20}$$

Twisting torque

The torque on the ith segment induced by twisting the $(i + 1)$th segment by an angle τ_{i+1} with respect to the ith one is

$$\frac{T_{i,\mathrm{next}}^{(t)}}{k_B T} = \frac{C}{k_B T l_0}\tau_{i+1} \tag{21}$$

The total twisting torque for the ith segment is then

$$T_i^{(t)} = -T_{(i-1),\mathrm{next}}^{(t)} + T_{i,\mathrm{next}}^{(t)} \tag{22}$$

Electrostatic force

The contribution of the electrostatic interaction between segments i and j to the force acting on the ith vertex is

$$\frac{\mathbf{F}_{ij,1}^{(e)}}{k_B T} = -\frac{1}{k_B T}\frac{\partial E_{ij}^{(e)}}{\partial \mathbf{r}_i} = \alpha_e\left(\frac{\partial f_{ij}}{\partial \rho_{ij}}\frac{\partial \rho_{ij}}{\partial \mathbf{r}_i} + \frac{\partial f_{ij}}{\partial \gamma_{ij}}\frac{\partial \gamma_{ij}}{\partial \mathbf{r}_i} + \frac{\partial f_{ij}}{\partial \gamma_{ji}}\frac{\partial \gamma_{ji}}{\partial \mathbf{r}_i} + \frac{\partial f_{ij}}{\partial \sigma_{ij}}\frac{\partial \sigma_{ij}}{\partial \mathbf{r}_i}\right)$$

where $f_{ij} = f(\rho_{ij}, \gamma_{ij}, \gamma_{ji}, \sigma_{ij})$. An analogous relationship is valid for the force $\mathbf{F}_{ij,2}^{(e)}$ acting on the $(i + 1)$th vertex from segment j. We assume that $\mathbf{F}_{ij,3}^{(e)} = \mathbf{F}_{ij,2}^{(e)} = 0$ when $i = j$ or $i = j \pm 1$. The partial derivatives of f (Eq. 8) are tabulated as described above. The expressions for the derivatives of ρ_{ij}, γ_{ij}, γ_{ji}, and σ_{ij} with respect to $\mathbf{r}_i$ and $\mathbf{r}_{i+1}$ are given below, where the following auxiliary notations are used: $\hat{\mathbf{R}}_{ij} = \mathbf{R}_{ij}/\rho_{ij}$ is a unit vector in the $\mathbf{R}_{ij}$ direction; $\alpha_{i(j)}$ and $\beta_{i(j)}$ are the coefficients in the expression for the "shifted" middle-point of a segment:

$$r_{i(j)}^{(m)} = \alpha_{i(j)} r_i + \beta_{i(j)} r_{i+1},$$

so that (see Eq. 11):

$$\alpha_{i(j)} = (1/2)(1 \pm (1 - l_0/s_i));$$

$$\beta_{i(j)} = (1/2)(1 \mp (1 - l_0/s_i))$$

The upper variant corresponds to the condition (a) in Eq. 11, the lower variant corresponds to the condition (b).

The partial derivatives are thus:

$$\frac{\partial \rho_{ij}}{\partial \mathbf{r}_i} = -\frac{1}{l_0}\alpha_{i(j)}\hat{\mathbf{R}}_{ij} \mp \frac{1}{2}\frac{\gamma_{ij}}{s_i}\mathbf{e}_i \tag{23}$$

$$\frac{\partial \rho_{ij}}{\partial \mathbf{r}_{i+1}} = -\frac{1}{l_0}\beta_{i(j)}\hat{\mathbf{R}}_{ij} \pm \frac{1}{2}\frac{\gamma_{ij}}{s_i}\mathbf{e}_i \tag{24}$$

$$\frac{\partial \gamma_{ij}}{\partial \mathbf{r}_i} = \frac{1}{s_i}(\gamma_{ij}\mathbf{e}_i - \hat{\mathbf{R}}_{ij}) - \frac{1}{\rho_{ij}}\left[\frac{1 \pm 1}{2l_0}\mathbf{e}_i + \gamma_{ij}\frac{\partial \rho_{ij}}{\partial \mathbf{r}_i}\right] \tag{25}$$

$$\frac{\partial \gamma_{ij}}{\partial \mathbf{r}_{i+1}} = -\frac{1}{s_i}(\gamma_{ij}\mathbf{e}_i - \hat{\mathbf{R}}_{ij}) - \frac{1}{\rho_{ij}}\left[\frac{1 \mp 1}{2l_0}\mathbf{e}_i + \gamma_{ij}\frac{\partial \rho_{ij}}{\partial \mathbf{r}_{i+1}}\right] \tag{26}$$

$$\frac{\partial \gamma_{ji}}{\partial \mathbf{r}_i} = \frac{1}{\rho_{ij}}\left[\frac{1}{l_0}\alpha_{i(j)}\mathbf{e}_j \pm \frac{(\mathbf{e}_i \cdot \mathbf{e}_j)}{2s_i}\mathbf{e}_i - \gamma_{ji}\frac{\partial \rho_{ij}}{\partial \mathbf{r}_i}\right] \tag{27}$$

$$\frac{\partial \gamma_{ji}}{\partial \mathbf{r}_{i+1}} = \frac{1}{\rho_{ij}}\left[\frac{1}{l_0}\beta_{i(j)}\mathbf{e}_j \mp \frac{(\mathbf{e}_i \cdot \mathbf{e}_j)}{2s_i}\mathbf{e}_i - \gamma_{ji}\frac{\partial \rho_{ij}}{\partial \mathbf{r}_{i+1}}\right] \tag{28}$$

$$\frac{\partial \sigma_{ij}}{\partial \mathbf{r}_i} = \sqrt{1 - \sigma_{ij}^2}\left\{\frac{s_j\gamma_{ji}}{|\hat{\mathbf{R}}_{ij} \times \mathbf{s}_j|^2\rho_{ij}}\left[\frac{1}{l_0}\alpha_{i(j)}(\hat{\mathbf{R}}_{ij} \times \mathbf{s}_j) \pm \frac{1}{2}\frac{(\hat{\mathbf{R}}_{ij} \cdot (\mathbf{s}_i \times \mathbf{s}_j))}{s_i^2}\mathbf{e}_i\right] - \frac{\hat{\mathbf{R}}_{ij} \times \mathbf{s}_i}{|\hat{\mathbf{R}}_{ij} \times \mathbf{s}_i|^2}\left(1 - \frac{\alpha_{i(j)}s_i\gamma_{ij}}{l_0\rho_{ij}}\right)\right\}; \tag{29}$$

$$\frac{\partial \sigma_{ij}}{\partial \mathbf{r}_{i+1}} = \sqrt{1 - \sigma_{ij}^2}\left\{\frac{s_j\gamma_{ji}}{|\hat{\mathbf{R}}_{ij} \times \mathbf{s}_j|^2\rho_{ij}}\left[\frac{1}{l_0}\beta_{i(j)}(\hat{\mathbf{R}} \times \mathbf{s}_j) \mp \frac{1}{2}\frac{(\hat{\mathbf{R}}_{ij} \cdot (\mathbf{s}_i \times \mathbf{s}_j))}{s_i^2}\mathbf{e}_i\right] - \frac{\hat{\mathbf{R}}_{ij} \times \mathbf{s}_i}{|\hat{\mathbf{R}}_{ij} \times \mathbf{s}_i|^2}\left(1 + \frac{\beta_{i(j)}s_i\gamma_{ij}}{l_0\rho_{ij}}\right)\right\}; \tag{30}$$

In Eqs. 29 and 30 the positive value of the square root $\sqrt{1 - \sigma_{ij}^2}$ is taken when $\mathbf{R}_{ij} \cdot (\mathbf{s}_i \times \mathbf{s}_j) > 0$, and its negative value otherwise.

The total electrostatic force acting on the ith vertex is

$$\mathbf{F}_i^{(e)} = \sum_{j=0}^{N-1}(\mathbf{F}_{ij,1}^{(e)} + \mathbf{F}_{(i-1)j,2}^{(e)}) \tag{31}$$

The boundary conditions for the force expressions, Eqs. 12–31, are different for linear and circular chains. For a linear chain all parameters with indexes out of range do not exist and can be formally set to zero. The allowed ranges are $0 \le i \le N - 1$ for $\mathbf{F}_{i,\mathrm{next}}^{(s)}$, $T_{i,\mathrm{next}}^{(t)}$; $1 \le i \le N - 1$ for $\mathbf{F}_{i,\mathrm{next}}^{(b)}$, $\mathbf{F}_{i,\mathrm{prev}}^{(b)}$, $T_i^{(b)}$, $\mathbf{F}_{i,\mathrm{next}}^{(t)}$, $\mathbf{F}_{i,\mathrm{prev}}^{(t)}$; $0 \le i \le N - 1$, $0 \le j \le N - 1$ for $\mathbf{F}_{ij,1}^{(e)}$, $\mathbf{F}_{ij,2}^{(e)}$. For a closed circular chain circular boundary conditions are in effect, such that all indices have to be taken modulo N.

Hydrodynamic interactions

In order to model hydrodynamic interactions defined between spherical objects, a bead with radius a was attached to each chain vertex. With $N' = N + 1$ beads for a linear and $N' = N$ beads for a circular chain, we describe the hydrodynamic interaction between beads i and j by a 3×3 Rotne-Prager tensor:

$$D_{ij} = D_0\frac{3a}{4r_{ij}}\left[I + \frac{r_{ij} \otimes r_{ij}}{r_{ij}^2} + \frac{2a^2}{3r_{ij}^2}\left(I - 3\frac{r_{ij} \otimes r_{ij}}{r_{ij}^2}\right)\right], \quad \text{if } r_{ij} \ge 2a,\ i \ne j; \tag{32a}$$

$$D_{ij} = D_0\left[\left(1 - \frac{9}{32}\frac{r_{ij}}{a}\right)I + \frac{3}{32}\frac{r_{ij} \otimes r_{ij}}{ar_{ij}}\right], \quad \text{if } r_{ij} \le 2a,\ i \ne j; \tag{32b}$$

$$D_{ii} = D_0 I \tag{32c}$$

where $r_{ij} = r_j - r_i$, $r_{ij} = |r_{ij}|$, $D_0 = k_B T/6\pi\eta a$, η is the water viscosity, I is a unit 3×3 matrix, and $r \otimes r$ denotes a matrix with the components $(r_\alpha r_\beta)$; $\alpha, \beta = x, y, z$.

The bead radius a is connected with the DNA hydrodynamic radius r_{HD} in the following way. Let us consider two

(a) (b)

Moteurs de jeu/de physique : Open Dynamics Engine

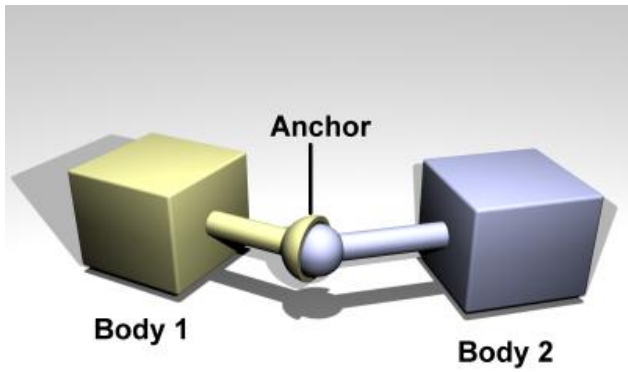

(a) joint ball

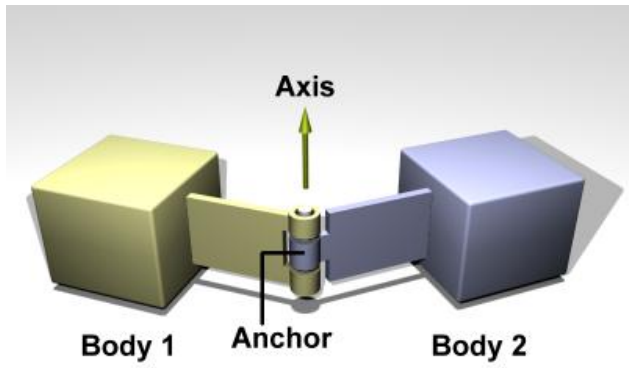

(b) joint hinge

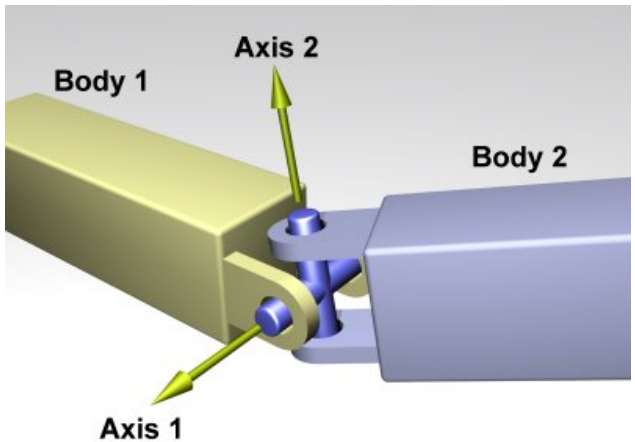

(c) joint universal

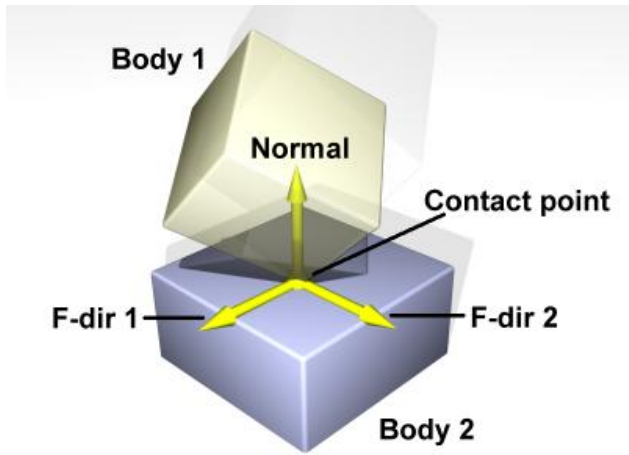

(d) joint de contact

FIGURE: Les joints dans ODE (R. Smith) sont des contraintes holonomiques.

Modèle mécanique d'ADN

1. Cylindre de longueur l et de rayon r
2. Rayon effectif $d^\star = d_c + l_D$
3. $r_c = 1\ \mathrm{nm}$ rayon crystallographique de l'ADN, l_D longueur de Debye
4. Dynamique de Langevin-Euler optimisée pour des corps rigides
   $\dot{\boldsymbol{\mathcal{L}}} = \boldsymbol{\mathcal{F}} + \Sigma^\star \left[\frac{\langle E \rangle}{E} \left(1 - \frac{1}{2\beta \langle E \rangle} \right) - 1 \right] \boldsymbol{\mathcal{L}} dt + \sqrt{\frac{\Sigma^\star}{\beta E}} \boldsymbol{\mathcal{L}} \frac{d\mathcal{W}}{dt}$
5. Dynamique de Langevin-Euler optimisée (vidéo)
6. Couples de courbure et de twist $\boldsymbol{\Gamma}_{b,t} = g_b \mathbf{t}_1 \times \mathbf{t}_2 + \frac{g_t \phi}{1+\cos\theta} (\mathbf{t}_1 + \mathbf{t}_2)$

Calibration des longueurs de persistance

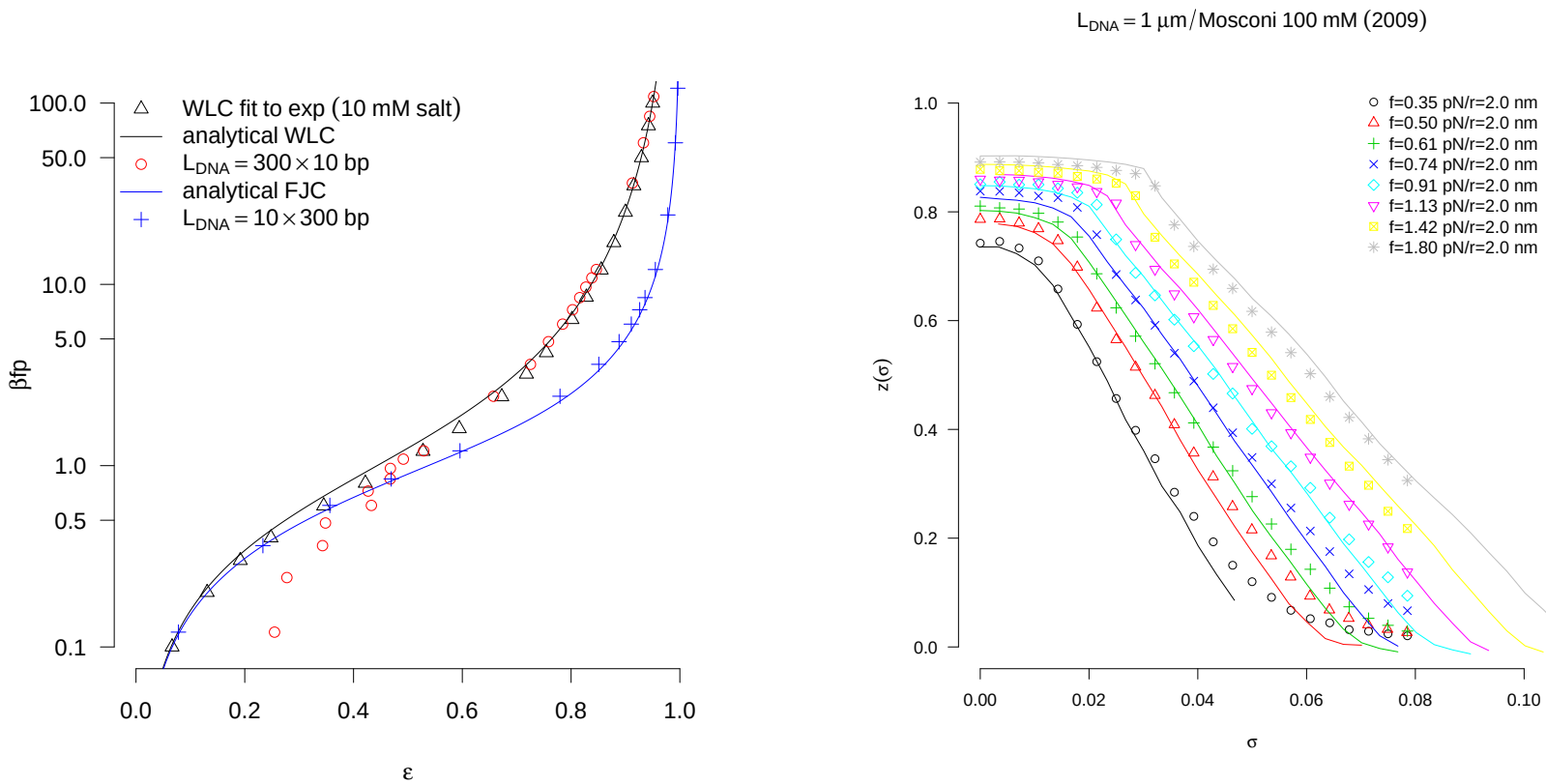

(a) Force extension

(b) Extension rotation

FIGURE: Paramètres des simulations $p = 50$ nm, $t = 95$ nm, et $L_{ADN} = 1$ µm

Instabilité de buckling

Extension, rotation en fonction du temps

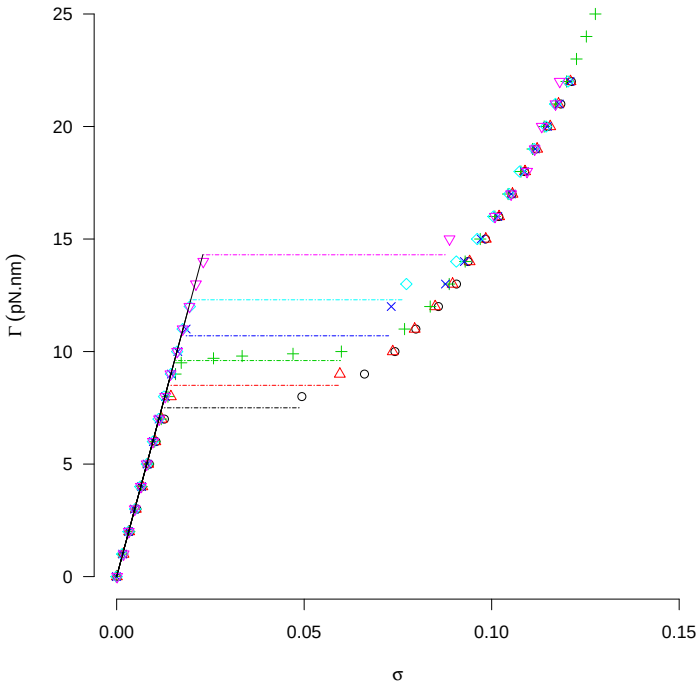

(a) Couple rotation

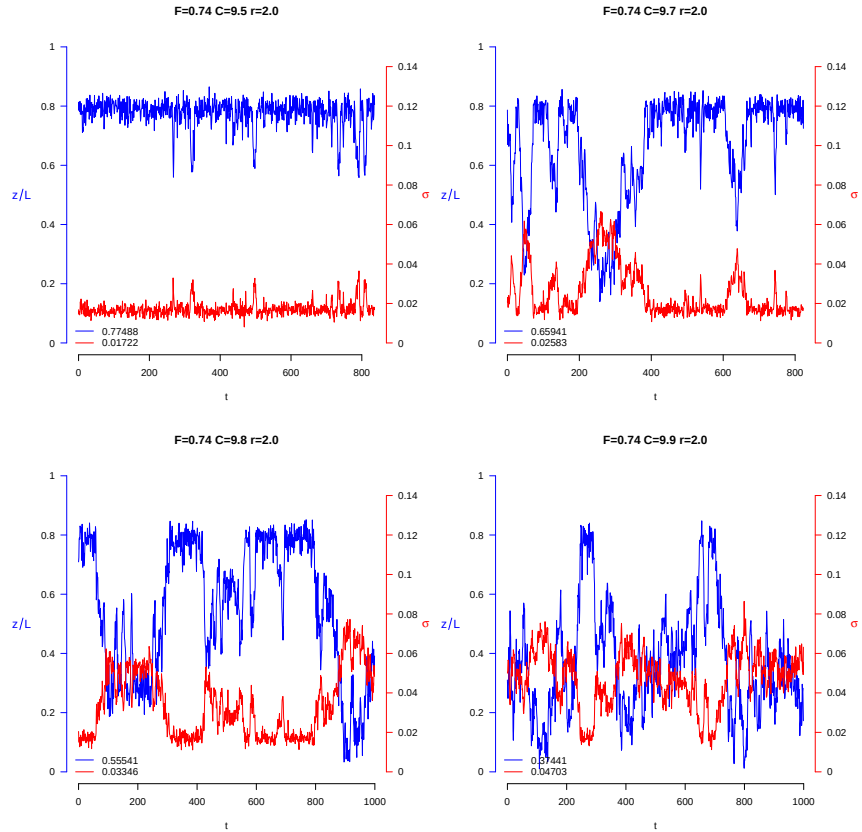

(b) Extension, rotation en fonction du temps

FIGURE: Paramètres des simulations $p = 50$ nm, $t = 95$ nm, et $L_{ADN} = 1$ µm.

Pinces magnétiques et fibre de chromatine

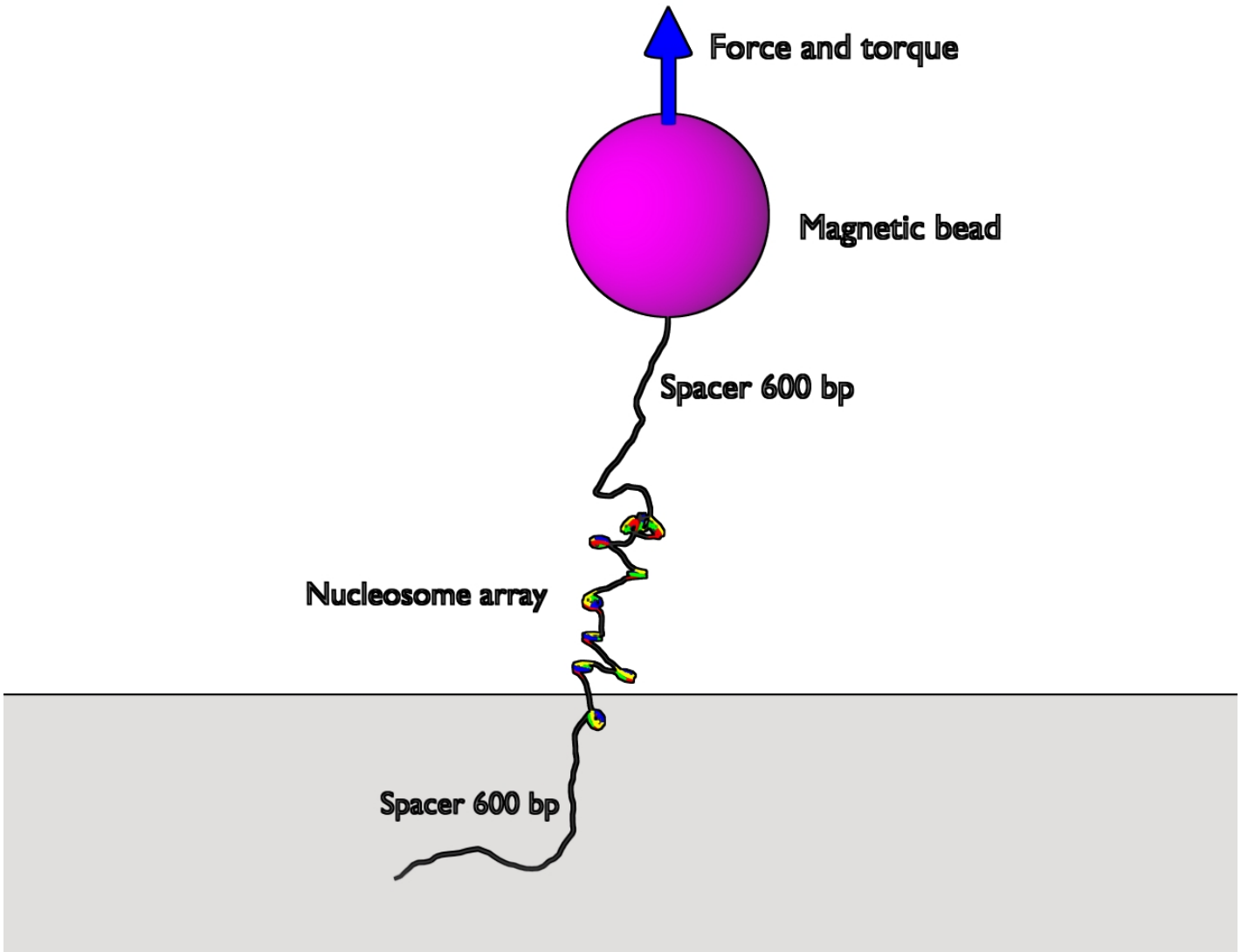

Modèle géométrique coarse-grained du nucléosome

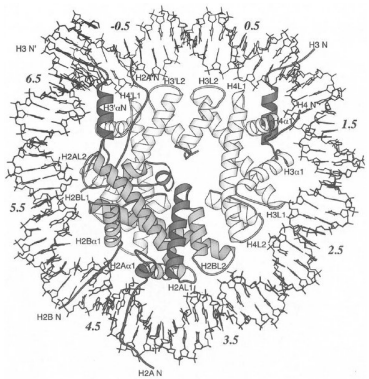

(a) Luger 1998

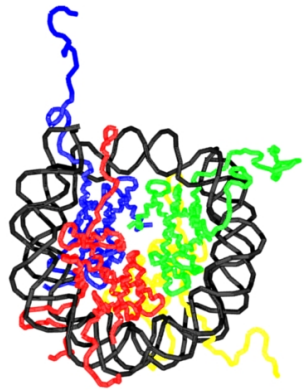

(b) Structure crystallographique 1KX5.pdb

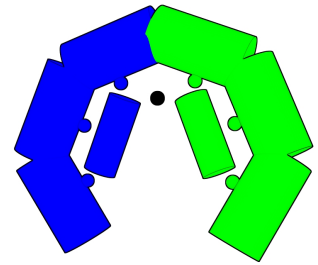

(c) Tétrasome

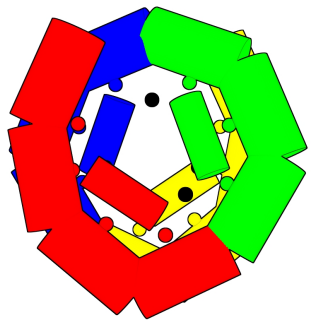

(d) Nucléosome fermé

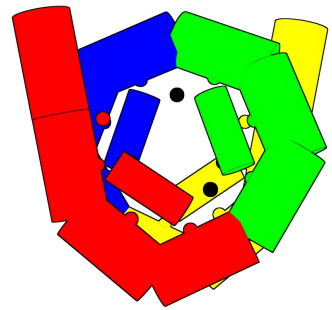

(e) Nucléosome ouvert

FIGURE: Vue schématique du modèle de nucléosome. L'ADN nucléosomale est enroulé à gauche. (Rouge et jaune) dimères H2A-H2B. (Bleu et vert) dimères H3-H4, HmfA et HmfB pour les archaea. (Noir) Four-Helix-Bundle. L'énergie de liaison des SHLs 6.5 est de l'ordre de l'agitation thermique.

Quelques vidéos pour conclure

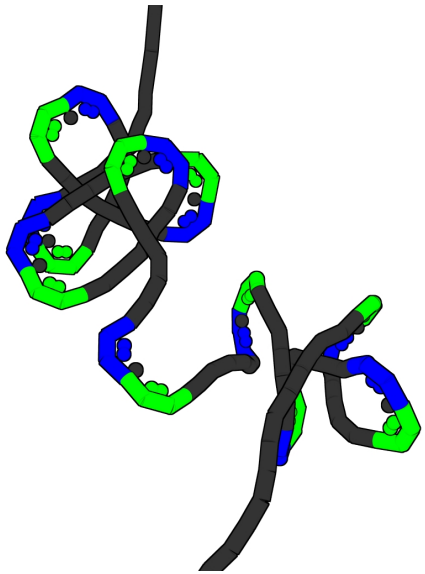

(a) Filament de 10 tétrasomes

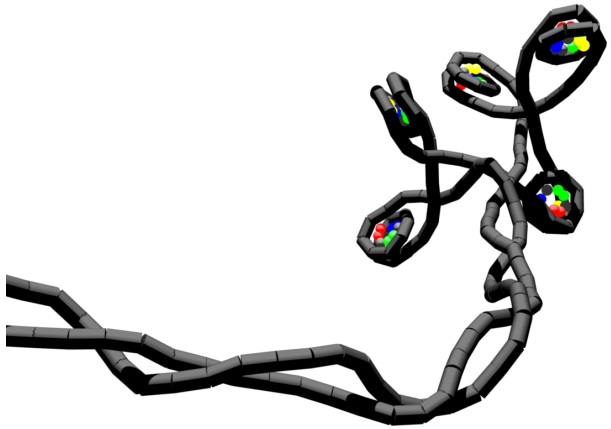

(b) Filament de nucléosomes avec plectonemes

Mélange (vidéo)
Réversome : force de traction $f = 3.0\ \mathrm{pN}$, couple $\Gamma = 25\ \mathrm{pN \cdot nm}$ (vidéo)
Fibre : force de traction $f = 0.3\ \mathrm{pN}$, couple $\Gamma = 6\ \mathrm{pN \cdot nm}$ (vidéo)
Fibre : force de traction $f = 0.3\ \mathrm{pN}$, couple $\Gamma = 10\ \mathrm{pN \cdot nm}$ (vidéo)
Fibre de 10 nucléosomes : force de traction $f = 3\ \mathrm{pN}$ (vidéo)